Spatial distribution of cluster size and density in supersonic jets as targets for intense laser pulses

F. Dorchies,[1] F. Blasco,[1] T. Caillaud,[1] J. Stevefelt,[1] C. Stenz,[1] A. S. Boldarev,[2] and V. A. Gasilov[2]
[1]*CELIA, UMR 5107 CNRS–Université Bordeaux 1, 33405 Talence, France*
[2]*Institute of Mathematical Modeling, Russian Academy of Sciences, Moscow 125047, Russia*
(Received 30 December 2002; published 27 August 2003)

Clusters were produced as a result of argon gas cooling during expansion through a supersonic nozzle. A two-dimensional model was set up in order to calculate gas expansion and partial condensation into clusters. Calculations were validated by experimental measurements using Mach-Zehnder interferometry and Rayleigh scattering, and performed with two types of nozzles (Laval and conical nozzles). These optical diagnostics together with numerical simulations led to the cluster size and density determination with spatial resolution through the gas and cluster jet. Cluster production was observed to be very sensitive to the nozzle geometry. Homogeneous gas and cluster jets were produced and characterized using conical nozzle geometry, with cluster density about 10^{12} per cm^3. Due to the fast valve-nozzle connecting geometry, shock waves have been observed at the Laval nozzle throat that strongly affected cluster production on the jet axis. Averaged cluster radius was observed to be easily tunable from 180 to 350 Å by varying the upstream gas pressure P_0 from 20 to 60 bars. A different scaling law, versus P_0, has been observed for this regime of large cluster, compared to Hagena's predictions for the small cluster regime.

DOI: 10.1103/PhysRevA.68.023201 PACS number(s): 36.40.−c, 64.70.Fx, 52.50.Jm

I. INTRODUCTION

A great interest in clusters has been observed in the past few years, as a target for intense laser interaction with matter (see, for example, the overview in Ref. [1]). Clusters produced from rare-gas cooling in supersonic expansion have been shown to constitute an intermediate state of matter that combines advantages of gas targets with an absorption efficiency that is even higher than that of solid targets [2]. A number of groups have been motivated by the possibility of using clusters to produce high-temperature plasmas for fundamental plasma physics [3], as well as for strong bursts of energetic particles such as x rays [4] or neutrons [5]. Such a new laser-matter interaction regime has been proposed to provide debris-free sources of soft x rays for the next generation lithography [6].

Understanding of basic phenomena involved in laser-cluster interaction relies on the knowledge about the target. To get information about the unique cluster response with given initial parameters, it is necessary to characterize and control cluster size as well as their spatial distribution through the jet. Most of the published experimental work has been performed with cluster jets produced with a nozzle and skimmers (see, e.g., Ref. [7]). With this geometry, an empirical formula was proposed by Hagena [8,9] in order to estimate the average cluster size as a function of an introduced parameter Γ^*, which depends on nozzle and upstream gas parameters:

$$N = 33\left(\frac{\Gamma^*}{1000}\right)^{2.35},$$

where N is the average number of atoms per cluster. This formula first established from mass spectrometer measurements [9] was then confirmed via different techniques including high-energy electron diffraction [10], He atom scattering [11], and Rayleigh scattering [12,13] on argon clusters. A similar scaling law was also obtained with a geometry without skimmers allowing cluster jets of higher density [14]. Depending on the technique used, agreement on absolute or relative values was only obtained in the range $\Gamma^* \leqslant 10^4$. That means for argon, clusters containing less than $N \sim 10^4$ atoms. Besides, the size given by this formula was spatially integrated through the jet, and no information was available about the cluster density and spatial distribution through the jet. Such an information is crucial to determine the number of clusters in the focal volume irradiated by a laser pulse.

A two-dimensional model was built in order to calculate the gas expansion and condensation into clusters through the nozzle [15,16]. In this paper, this model is presented in detail and compared with experimental measurements using Mach-Zehnder interferometry and Rayleigh scattering. A special effort was made to measure spatially resolved absolute values. Good agreement was observed. Optical diagnostics together with numerical simulations led to a determination of the cluster size and density, with spatial resolution through the gas and cluster jet. The nozzle geometry was observed to significantly affect the spatial distribution of clusters. Two different types of nozzles were studied (Laval and conical nozzles) with upstream pressure from 20 to 60 bars. In this regime of large clusters, the Hagena parameter Γ^* varied from 10^4 to 10^6, extending the range already experimentally validated.

II. DEFINITIONS AND EXPERIMENTAL APPARATUS

The target is a two-phase system, composed of argon gas and clusters expanding in a vacuum chamber. The clusters studied in this paper contain more than 1000 atoms, and in this range, their structure has been determined to be crystalline fcc with a lattice parameter $a = 5.34 \pm 0.01$ Å [17]. Thus, the radius r (Å) of a cluster composed of n atoms is given by

$$r \approx \sqrt[3]{9n} \quad \Leftrightarrow \quad n(r) \approx \frac{r^3}{9}. \tag{1}$$

Assuming the two-phase system to be in a stationary state, it can be described at each spatial location $\mathbf{x}$ by the following parameters: (1) the total atomic density $N_{\mathrm{tot}}(\mathbf{x})$ (i.e., including all atoms both in gas and cluster phases), (2) the condensation degree $\eta(\mathbf{x})$ (i.e., the fraction of atoms under cluster phase), (3) the distribution function $f(r,\mathbf{x})$ of the clusters with respect to their radii r.

In this paper, we use experimental and computational methods to determine spatially resolved but statistically averaged parameters (i.e., averaged over the distribution function f). Several physical parameters can be defined such as the cluster density N_{clus}, the average cluster radius R, or the average number of atoms per cluster N. They are, respectively, obtained from

$$N_{\mathrm{clus}}(\mathbf{x}) = \int_0^\infty f(r,\mathbf{x})dr,$$

$$R(\mathbf{x}) = \int_0^\infty r f(r,\mathbf{x})dr \Big/ \int_0^\infty f(r,\mathbf{x})dr,$$

$$N(\mathbf{x}) = \int_0^\infty n(r) f(r,\mathbf{x})dr \Big/ \int_0^\infty f(r,\mathbf{x})dr.$$

N and N_{clus} are related by

$$N N_{\mathrm{clus}} = \eta N_{\mathrm{tot}}. \tag{2}$$

Neglecting the standard deviation of cluster radius distribution, N and R could be related by Eq. (1). Nevertheless, it should be noted that this is not *strictly* the case, since the distribution function f is not a Dirac function. Under these considerations, the two-phase system can be completely described by a set of three independent local parameters: $N_{\mathrm{tot}}(\mathbf{x})$, $\eta(\mathbf{x})$, and $N(\mathbf{x})$ for example, or $N_{\mathrm{tot}}(\mathbf{x})$, and $R(\mathbf{x})$.

The study presented in this paper was performed with two types of nozzles currently used in experiments of laser interaction with cluster jets: Laval nozzle (left part of Fig. 1) and conical nozzle (right part of Fig. 1). They are both composed of a commercial electrovalve [18] and the nozzle in itself. The Laval nozzle consists of a first convergent conical part down to a $\phi_w = 820 \pm 20$ μm diameter throat, followed by a parabolic divergent part. The $\phi_{\mathrm{out}} = 2.40 \pm 0.05$ mm diameter output section is separated by a distance of $L = 13.0 \pm 0.1$ mm from the throat section. The conical nozzle consists in a first convergent conical part down to a $\phi_w = 620 \pm 20$ μm diameter throat, followed by a conical divergent part. The $\phi_{\mathrm{out}} = 3.80 \pm 0.05$ mm diameter output section is separated by a distance of $L = 20.2 \pm 0.1$ mm from the throat section. These two nozzles are both made with axial symmetry. Gas expansion and cluster production are consequently supposed to have a revolution symmetry around the nozzle axis. The jet was controlled by an electromagnetic valve pulsed with a variable opening time. The upstream pressure

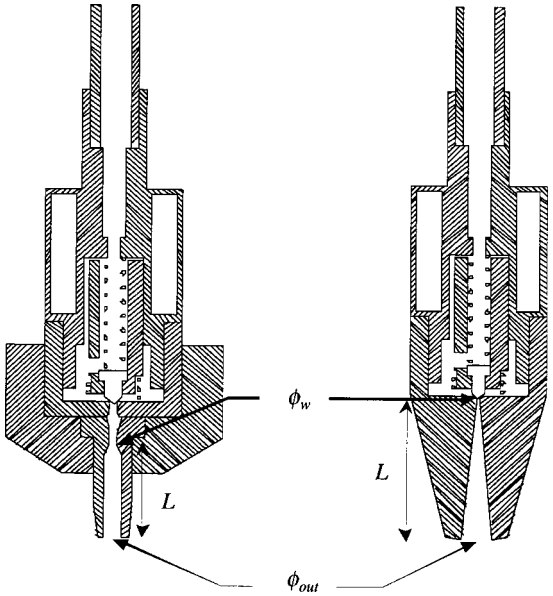

FIG. 1. Sketch of the two nozzles studied. They are both composed of a commercial electrovalve [17] and the nozzle in itself. Right: conical nozzle (diameters $\phi_w = 620$ μm, $\phi_{\mathrm{out}} = 3.8$ mm, and length $L = 20.2$ mm). Left: the Laval nozzle (diameters $\phi_w = 820$ μm, $\phi_{\mathrm{out}} = 2.4$ mm, and length $L = 13.0$ mm).

P_0 of the nozzles was varied and controlled by a precise pressure gauge. The setup was at room temperature (i.e., $T_0 = 293$ K).

III. SIMPLE ONE-DIMENSIONAL ESTIMATE OF THE GAS FLOW PARAMETERS

The gas expansion into the divergent part of a Laval nozzle or a conical divergent nozzle can be analytically described within a one-dimensional (1D) model if we do not take into account gas condensation, viscosity, and also shock wave formation into the nozzle. This approach is not relevant to determine spatial distributions at the nozzle output. But it presents a simple way to estimate the total atomic density, the mass flux, and the ability of cluster production in the stationary regime. At each point along the nozzle, the gas flow is described by parameters such as pressure P, mass density ρ, gas temperature T, and flow velocity v. Considering the adiabatic expansion of a perfect gas in a given nozzle profile, they are related by the well-known gasdynamics relations:

$$P = \frac{\rho k_B T}{m},$$

$$P \rho^{-\gamma} = \mathrm{const},$$

$$S v \rho = \mathrm{const},$$

$$\int \frac{dP}{\rho} + \frac{v^2}{2} = \mathrm{const},$$

m is the atomic mass, k_B is the Boltzmann constant, S is the nozzle section, and γ is the ratio of the specific heats ($\gamma = \frac{5}{3}$ for monoatomic gas such as argon, $\gamma = \frac{7}{5}$ for diatomic gas). The last of these relations is the generalized Bernouilli equation (see, e.g., Ref. [19]).

From these relations, one can easily obtain gas parameters as a function of its initial values P_0, ρ_0, and T_0 (initial flow velocity $v_0 = 0$). At the nozzle throat, the gas flow velocity v_{thr} equals the local sound speed c_{thr}:

$$v_{\mathrm{thr}} = c_{\mathrm{thr}} = \left(\frac{dP}{d\rho}\right)_{\mathrm{thr}}^{1/2} = \left(\frac{\gamma k_B T_{\mathrm{thr}}}{m}\right)^{1/2} = \left(\frac{2}{\gamma+1}\right)^{1/2} c_0 .$$

c_0 is the sound speed calculated at the initial temperature T_0. Pressure P_{thr}, mass density ρ_{thr}, and temperature T_{thr} are given by

$$\left(\frac{P_{\mathrm{thr}}}{P_0}\right)^{(\gamma-1)/\gamma} = \left(\frac{\rho_{\mathrm{thr}}}{\rho_0}\right)^{(\gamma-1)} = \frac{T_{\mathrm{thr}}}{T_0} = \frac{c_{\mathrm{thr}}^2}{c_0^2} = \frac{2}{\gamma+1}.$$

At the nozzle output, the respective physical quantities are noted v_{out}, P_{out}, ρ_{out}, and T_{out}. Under the condition $\rho_{\mathrm{out}} \ll \rho_0$, the gas velocity is given by the simple following expression:

$$v_{\mathrm{out}} = \left(\frac{2}{\gamma-1}\right)^{1/2} c_0 .$$

As a consequence, the Mach number $M_{\mathrm{out}} = v_{\mathrm{out}}/c_{\mathrm{out}}$ at the nozzle output is given by

$$M_{\mathrm{out}} = \left[\left(\frac{\gamma+1}{\gamma-1}\right)^{(\gamma+1)/2}\right]^{1/2} \left(\frac{S_{\mathrm{out}}}{S_{\mathrm{thr}}}\right)^{(\gamma-1)/2}.$$

Other gas parameters can be simply related to the ratio between the output and throat nozzle sections, $S_{\mathrm{out}}/S_{\mathrm{thr}}$:

$$\left(\frac{P_{\mathrm{out}}}{P_0}\right)^{(\gamma-1)/\gamma} = \left(\frac{\rho_{\mathrm{out}}}{\rho_0}\right)^{(\gamma-1)} = \frac{T_{\mathrm{out}}}{T_0} = \frac{c_{\mathrm{out}}^2}{c_0^2} = \left(\frac{2}{\gamma-1}\right)\frac{1}{M^2}$$
$$= 2\left[\frac{(\gamma-1)^{\gamma-1}}{(\gamma+1)^{\gamma+1}}\right]^{1/2} \left(\frac{S_{\mathrm{thr}}}{S_{\mathrm{out}}}\right)^{\gamma-1}.$$

It should be noted that the condition $\rho_{\mathrm{out}} \ll \rho_0$ falls down to the equivalent condition $S_{\mathrm{thr}}/S_{\mathrm{out}} \ll 1$.

In the case of a no-clustering gas jet, this analytical model gives a good value of the output mass density. As experimentally and numerically demonstrated in the following part of this paper, this can be used with a good approximation to estimate the total atomic density, even in the case of a cluster jet. For a pulsed nozzle, a stationary regime can be assumed after the time needed for the fast valve to open and the time needed for the gas to reach the nozzle output $\sim L/c_0$. In our case, stationary regime was achieved after a time of the order of 500 μs, for a Laval nozzle at room temperature and $L = 2$ cm. Gas to liquid phase transition is not taken into account in the model. Nevertheless, it can be expected to occur if the output temperature calculated is lower than the saturation temperature. This simple calculation gives a simple way to estimate if the experimental device allows cluster production. One should also keep in mind that shock waves are not taken into account. They could decrease the Mach number achieved at the nozzle output, affecting the cluster production. A two-dimensional description of gas expansion and cluster production with an appropriate numerical simulation is needed.

IV. MATHEMATICAL MODEL OF CLUSTER PRODUCTION

The numerical method used to calculate gas supersonic expansion as well as cluster production is described in previous papers [15,16]. The detailed presentation of the theory of spontaneous condensation can be found, for example, in Ref. [20]. An application of the classical condensation theory to jets is given by Bartell (see, e.g., Ref. [21]). A different approach has been carried out by Garret and co-workers (see, e.g., Ref. [22]). In the simplest approach we used, the distribution function $f(r,\mathbf{x},t)$ of the clusters with respect to their radii r is represented by its moments:

$$\rho\Omega_n = \int_0^\infty f r^n dr, \quad n = 0,1,2, \ldots .$$

With this representation, the equations that govern the system composed by gas and clusters are the following:

$$\frac{\partial \rho}{\partial t} + \boldsymbol{\nabla}\cdot(\rho \boldsymbol{v}) = 0, \tag{3}$$

$$\frac{\partial \rho \boldsymbol{v}}{\partial t} + \boldsymbol{\nabla}\cdot(\rho \boldsymbol{v}\otimes \boldsymbol{v}) = -\boldsymbol{\nabla} P, \tag{4}$$

$$\frac{\partial}{\partial t}\left(\rho\varepsilon + \rho\frac{\boldsymbol{v}^2}{2}\right) + \boldsymbol{\nabla}\cdot\left[\rho \boldsymbol{v}\left(\varepsilon + \frac{\boldsymbol{v}^2}{2}\right)\right] = -\boldsymbol{\nabla}\cdot(P\boldsymbol{v}), \tag{5}$$

$$\frac{\partial \rho\Omega_0}{\partial t} + \boldsymbol{\nabla}\cdot(\rho \boldsymbol{v}\Omega_0) = I, \tag{6}$$

$$\frac{\partial \rho\Omega_n}{\partial t} + \boldsymbol{\nabla}\cdot(\rho \boldsymbol{v}\Omega_n) = I r_*^n + n\dot{r}\rho\Omega_{n-1} \quad (n = 1,2), \tag{7}$$

$$\frac{\partial \rho\beta}{\partial t} + \boldsymbol{\nabla}\cdot(\rho \boldsymbol{v}\beta) = -\tfrac{4}{3}\pi\rho_l r_*^3 I - 4\pi\rho\rho_l \dot{r}\Omega_2 . \tag{8}$$

ρ, $\boldsymbol{v}$, ε, and P are, respectively, the global density, velocity, specific internal energy, and pressure of the system. $\beta = 1 - \eta$ is the dryness, i.e., the mass quota of gas phase and ρ_l is the density of liquid phase.

The values of the moments in any point $\mathbf{x}$ can be derived from system (3)–(8), leading to the different cluster parameters. For example, the cluster concentration N_{clus} is obtained from

$$N_{\mathrm{clus}} = \rho\Omega_0 ,$$

the average radius R from

$$R=\frac{\Omega_1}{\Omega_0}, \quad \text{etc.}$$

The kinetics of cluster formation itself is described by the terms $\dot{r}$, r_*, and I, which are, respectively, the cluster growth rate, the critical radius, and the nucleation rate, on the right-hand sides of Eqs. (6)–(8). The following expressions are used for these parameters:

$$\dot{r}=\frac{P}{\rho_l\sqrt{2\pi R_g T}}\left[1-\left(\frac{T}{T_s(P)}\right)^{1/2}\right], \tag{9}$$

$$r_*=\frac{2\sigma}{\rho_l R_g T \ln(P/P_s)}, \tag{10}$$

$$I=\frac{1}{\rho_l}\left(\frac{2\sigma\mu}{\pi N_A}\right)^{1/2}\left(\frac{P}{k_B T}\right)^2 \exp\left(-\frac{4\pi\sigma r_*^2}{3k_B T}\right), \tag{11}$$

where $R_g=R_0/\mu$ is the gas constant, T is the actual temperature, $T_s(P)$ is the saturation temperature at pressure P, $P_s(T)$ is the saturation pressure, σ is the surface-tension coefficient, μ is the mass per mole, and N_A is the Avogadro number.

The expressions for I and r_* are taken from the classical theory of heterophase fluctuations presented by Frenkel [23]. This theory is based on the fact that a small liquid droplet can be in equilibrium with a supercooled gas, since the surface tension provides an additional potential barrier for a molecule depositing on the droplet. It leads to a definite value of critical radius r_* (i.e., at equilibrium) depending on supercooled gas parameters. Expression (10) for r_* is called Thomson's formula. It can be obtained by detailed calculation of numbers of molecules leaving and entering the droplet, or by the analysis of the chemical potential. The equilibrium of the critical droplet is unsteady, since a smaller droplet evaporates, while a larger droplet grows.

As a consequence, a condensation nucleus able of further growing can form if a cluster of critical size occasionally occurs due to molecular fluctuations. In order to evaluate the frequency of such events, the dynamics of subcritical clusters is considered within the classical theory of nucleation. The distribution of such subcritical clusters is supposed to be stationary, leading to expression (11) for I (Frenkel-Zeldovich formula). The experimental validation of the model remains necessary, since there are some doubts about the validity of the main suppositions of classical theory (macroscopic approach to all molecular clusters under consideration, stationary distribution of subcritical clusters).

To obtain the results of modeling, we solve the system of equations (3)–(8), closed by expressions (9)–(11), in the spatial domain including the inner cavity of the nozzle and some open space behind its outlet. Boundary conditions corresponding to the gas initial parameters are set at the inlet, and at the outlet, boundary conditions are set corresponding to vacuum. Then calculations are performed to achieve the stationary state. As a rule, the computations are carried out in a two-dimensional formulation with axial symmetry, leading to the two-dimensional distribution of all the values under consideration. One-dimensional computations can be performed too. They permit to evaluate the characteristic values of the parameters in the outlet section of the nozzle, with very little computer time in comparison with two-dimensional computations.

V. MACH-ZEHNDER INTERFEROMETRY DIAGNOSTIC

Argon jets were first studied by Mach-Zehnder interferometry using the gas jet facility at LULI (Laboratoire pour l'Utilisation des Lasers Intenses, Ecole Polytechnique, Palaiseau, France). The experimental setup is fully described in Ref. [24]. This Mach-Zehnder interferometer was based on a He-Ne laser divided in two arms by the use of a beam splitter. One of these arms propagated through vacuum, the other one propagated through the gas jet. A second beam splitter recombined the two arms that interfered. A lens imaged the gas jet plane, collecting interferograms on a CCD (charge-coupled device) camera. As the He-Ne laser was continuous but not the gas jet, an optical shutter was used with a 2 ms opening time. An electronic delay box was used to adjust the delay between the gas jet and the shutter.

The phase shift measured by this technique integrated the refractive index η_{opt} across the gas jet along the He-Ne propagation axis. Assuming an axial symmetry, an Abel transformation was operated in order to obtain the value of η_{opt} resolved in the three dimensions of space. Since the He-Ne optical wavelength was far from a resonance associated with the cluster structure, η_{opt} was simply the macroscopic result of the contributions of all Ar atoms both in gas and cluster phases. This is related to the total atomic density N_{tot} by the following expression:

$$\eta_{\text{opt}}^2-1=\beta N_{\text{tot}}, \tag{12}$$

where $\beta=2.10\times10^{-23}$ cm^3 is the Gladstone-Dale constant of Ar [25]. As a consequence, this technique provided a complete determination of N_{tot} in the three spatial dimensions at the nozzle output. The spatial resolution was limited to 15 μm by the imaging device. The temporal resolution was limited to 2 ms by the optical shutter minimum opening time.

VI. RAYLEIGH SCATTERING DIAGNOSTIC

In a second part, Ar jets were characterized using the Rayleigh scattering diagnostic. A linearly polarized continuous He-Ne laser beam was focused into the gas and cluster jet. A lens was placed at 90° both to the laser axis and the jet axis. It imaged the scattered light onto a cooled CCD camera. The relative position of the He-Ne beam and the jet was varied in order to obtain spatial resolution in the jet. Calibration measurements with static gas were performed with exactly the same setup in order to keep the same factor C between the scattered light intensity and the signal measured on the CCD. This factor C takes into account the collection angle as well as the optical system transmission and the CCD quantum efficiency.

Each atom, in gas or cluster phase, constitutes a dipole excited by the laser electric field. This dipole emits scattered radiation at the same wavelength as described, for example, in Ref. [26]. The scattered field phase is controlled by the

laser electric-field phase, and the scattered intensity I_{at} is related to the laser intensity I_0 by

$$I_{at}=C\alpha_{at}^2 I_0;$$

α_{at} is the atom polarizability. The scattered intensity of N atoms in gas phase is

$$I_N(\text{gas})=NC\alpha_{at}^2 I_0,$$

since they are randomly distributed in a large volume. In the cluster phase case, the same N atoms can be confined into a small volume. If the cluster radius r is small compared to the wavelength λ, then all atoms contribute with the same phase to the total scattered electric field, leading to the Rayleigh scattering cross section [27]:

$$I_N(\text{cluster})=N^2C\alpha_{at}^2 I_0.$$

In the Mie regime (i.e., $r\sim\lambda$), destructive interference can be observed as a function of the observation angle [26]. The scattering angular distribution study is a powerful diagnostic of radius for very large cluster. In the range $R\sim 100-300$ Å concerned in this paper, this technique would need vacuum ultraviolet light that would be largely absorbed by the gas and cluster jet.

Considering a single-size distribution of clusters, each containing N atoms, the total intensity locally scattered by the gas and cluster jet was given by

$$I_{tot}=(1-\eta)N_{tot}C\alpha_{at}^2 I_0+N_{clus}N^2C\alpha_{at}^2 I_0.$$

This scattered intensity was normalized to the value I_{gas} obtained with static gas at the total atomic density N_{tot} deduced from the Mach-Zehnder measurements. Using Eq. (2), this normalized quantity simplified as

$$I_{tot}/I_{gas}=(1-\eta)+\eta N\approx\eta N, \tag{13}$$

since the number N of atoms per cluster is quite large in the range of concern ($N\sim 10^5$ for radius $R\sim 100$ Å). In the actual case, this quantity was averaged on the cluster size distribution, giving

$$I_{tot}/I_{gas}=(1-\eta)+\frac{\int_0^\infty n^2(r)f(r)dr}{\int_0^\infty n(r)f(r)dr}\eta\approx\frac{\langle n^2\rangle}{\langle n\rangle}\eta=\tilde{N}\eta, \tag{14}$$

which is slightly different from the previous formula.

By coupling the Rayleigh and Mach-Zehnder diagnostics we get the product of the condensation rate by the number of atoms per cluster averaged as in Eq. (14). This corresponds to the intuitive idea of a scattered signal increasing both with the average size and the density of clusters. The spatial resolution was about 100 μm, limited by the beam size in the scattering area. Scattered signals were registered without any optical shutter, then integrated over the valve opening time (stationary regime) set to a value much larger than the valve rising time (transitory regime). The great sensitivity of the Rayleigh scattering on cluster size ensured a good contrast between the signal induced by clusters and the contribution of low-density residual gas present when the valve was closed.

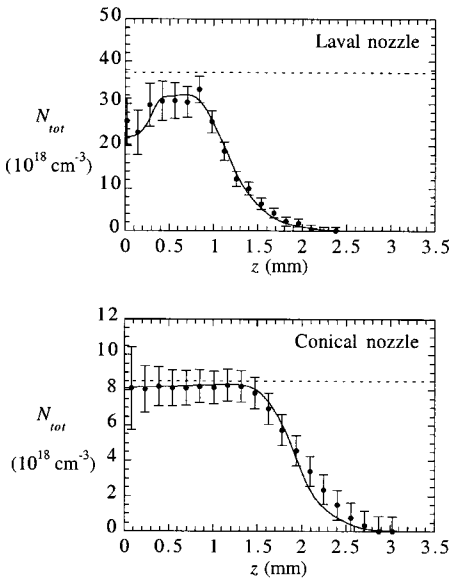

FIG. 2. Profiles of the total atomic density N_{tot} for the Laval nozzle (upper image) and conical nozzle (lower image) at 1.5 mm from the nozzle output with upstream pressure $P_0=40$ bars. Full line: 2D numerical calculation. Dotted line: 1D analytical calculation. Full circles: the Mach-Zehnder experiment. z is the distance from the jet axis.

VII. EXPERIMENTAL AND COMPUTED RESULTS

Profiles of total atomic density N_{tot} were obtained from the Mach-Zehnder measurements with the two nozzles described in Fig. 1, and with an upstream pressure P_0 in the range 10–100 bars. Calculations using the model presented in Sec. IV were performed at $P_0=20$, 40, and 60 bars. Profiles obtained with $P_0=40$ bars at 1.5 mm from the nozzle output are presented in Fig. 2 (Laval nozzle in the top image and conical nozzle in the bottom image) as a function of distance z from the jet axis. The error bars are larger near the axis, due to the Abel transformation. A very good agreement is observed between the experimental and numerical data. Shapes are very well reproduced and absolute values are the same within 10%. One should note that the value of N_{tot} obtained at the nozzle output from the 1D analytical calculation presented in Sec. III is also close to the value measured within 20%. In the case of the conical nozzle, the jet diameter measured at 1.5 mm from the nozzle output and defined as 10% of maximal density was observed to follow the expected spatial extent within the opening angle of the nozzle.

Similar profiles obtained with the Rayleigh diagnostic were compared with numerical calculations in the same pressure range and at the same distance 1.5 mm from the nozzle output. In Fig. 3, the measured quantity $\eta\tilde{N}N_{tot}$ (defined in Sec. VI) is plotted in the same graphs as the calculated quantity ηNN_{tot}, for $P_0=40$ bars. As in Fig. 2, the Laval nozzle corresponds to the upper part and the conical nozzle to the lower image. Absolute values of signal amplitude were well

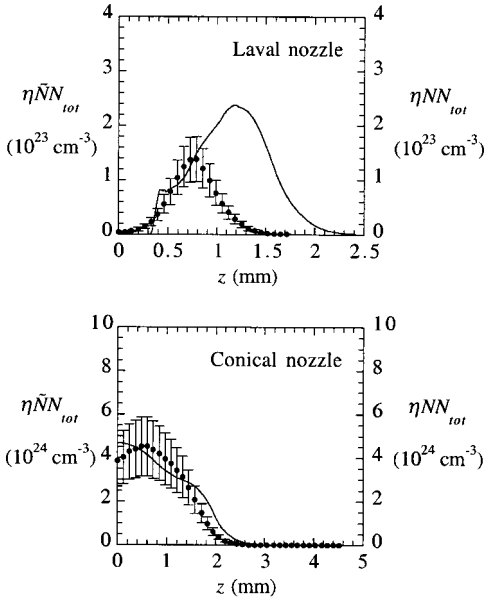

FIG. 3. Profiles of the quantity $\eta\tilde{N}N_{\mathrm{tot}}$ measured by the Rayleigh diagnostic, and compared with the calculated quantity ηNN_{tot} at 1.5 mm from the nozzle output. The upstream pressure was $P_0 = 40$ bars. Top image: the Laval nozzle. Bottom image: the conical nozzle. Full line: 2D numerical calculation. Full circles: experiment. z is the distance from the jet axis.

reproduced within 30%. The radial distribution of clusters was found to be annular (i.e., no clusters on jet axis) using the Laval nozzle, both numerically and experimentally. However, the mean radius of this annular distribution was 60% overestimated by calculation as compared to the measured value. Concerning the conical nozzle, a better agreement was found.

Laval nozzle calculations demonstrated large shock waves occurring at the very beginning of the gas expansion in association with the rapid section increase just after the nozzle throat. These shock waves converged and strongly affected both the Mach number and the condensation on the jet axis, leading to the annular cluster distribution observed [16]. As a consequence, very inhomogeneous profiles were obtained for both cluster radius and density, in terms of the distance z from the jet axis. In that sense, the Laval nozzle was determined not to be very suitable for fundamental laser-cluster experiments. Nevertheless, as larger atomic densities can be obtained with this nozzle than with the conical nozzle, the Laval nozzle seems to be more suitable for laser interaction experiments with high density and cluster-free gas target.

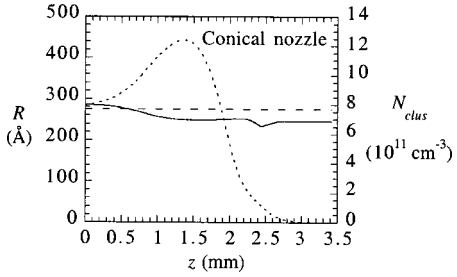

FIG. 4. Numerical profiles obtained with $P_0 = 40$ bars at 1.5 mm from the conical nozzle output, as a function of the distance z from the jet axis. Full line: cluster radius R. Dotted line: cluster density N_{clus}. Dashed line: cluster radius estimated at the nozzle output with 1D simulation.

Calculations performed at 40 bars, 1.5 mm from the nozzle output and at $z = 1.5$ mm from the jet axis led to a condensation rate η of the order of 10% and to a number N of atoms per cluster in the range of 5×10^4. This corresponds to a cluster radius $R\sim80$ Å and a cluster density $N_{\mathrm{clus}}\sim5\times10^{13}$ cm^{-3}.

As the section increase was smoother just after the throat, such shock waves have not been observed in conical nozzle calculations. Homogeneous profiles were determined for the different cluster parameters within the 4 mm jet diameter, indicating that this conical nozzle geometry is well suited for fundamental laser-cluster interaction experiments. Calculations performed with $P_0 = 40$ bars at 1.5 mm from the nozzle output led to higher condensation rate ($\eta\sim25\%$) and to bigger clusters ($N\sim2\times10^6$) as compared to the Laval nozzle. The corresponding profiles of cluster radius and density are plotted in Fig. 4, as functions of the distance z from the jet axis. Standard deviation δR of cluster size distribution was obtained from Eqs. (3)–(8), leading to $\delta R/R\sim12\%$. A 1D calculation based on the same equations as presented in Sec. IV was also performed for the nozzle output, and results are plotted in Fig. 4 together with the 2D calculation. This 1D calculation represented an interesting gain of time, and gave an estimation of the cluster average radius R in good agreement with the complete 2D calculation (i.e., within the calculated distribution width $\delta R/R$). Values of the different cluster parameters calculated from 1D numerical simulations are given in Table I. The cluster average radius was found to be adjustable from 180 to 350 Å by varying the upstream pressure P_0 from 20 to 60 bars.

VIII. DISCUSSION

The Mach-Zehnder experiment was performed as a function of the delay between the He-Ne laser probe and the

TABLE I. Cluster parameters calculated from 1D numerical simulations with upstream pressure P_0 from 20 to 60 bars. η is the condensation rate, R is the average cluster radius, $\delta R/R$ is the relative width of radius statistical distribution, N is the number of atoms per cluster, and N_{clus} is the cluster density.

P_0 (bars)	η (%)	R (Å)	$\delta R/R$ (%)	N	N_{clus} (cm^{-3})
20	20.7	183	14	6.14×10^5	1.60×10^{12}
40	23.5	275	12	1.97×10^6	1.12×10^{12}
60	25.3	348	11	3.87×10^6	9.20×10^{11}

valve opening. The signal was observed to reach its maximum value within the temporal resolution of the diagnostic. This indicated that a stationary regime was achieved within a time smaller than 2 ms after the valve opening. The same behavior was also observed at the valve closing. From analytical considerations (cf. Sec. III), 100 μs were expected for the gas to reach the nozzle output. The time needed for the valve to be opened was mechanically limited to 500 μs, and 1 ms to be closed. Comparable values of the front and back edge duration were already observed using the Rayleigh scattering [14]. Stationary regime should have been reached within the same time for cluster production, since condensation directly resulted from gas cooling during expansion. Absolute values of $\eta N N_{\mathrm{tot}}$ were deduced from the Rayleigh experiments by normalizing the signal, integrated during the 20 ms valve opening time. The error eventually induced by this averaging should not exceed 20% (8.5%), assuming 2 ms (600 μs) to reach and 2 ms (1.1 ms) to leave the stationary regime. In order to get a better estimation of this error, the Rayleigh scattering was measured with different valve opening time from 10 to 50 ms. Normalized signal was observed to depend linearly on the valve opening time. The difference between peak and average values inferred was found to be less than 5%.

Total atomic density profiles were fully determined by the Mach-Zehnder experiments. Nevertheless, the Rayleigh diagnostic was not able to disentangle η from N profiles, i.e., to determine separately the cluster size and density. Consequently, gas and cluster jets were characterized by the way of 2D numerical simulations based on the model presented in Sec. IV. Experiments were then used in order to validate these calculations. Within this approach, the 1D analytical model presented in Sec. III was observed to easily provide good values (i.e., 20% accuracy) for the total atomic density N_{tot}, up to 25% condensation rate. As shown in Fig. 4, cluster size, and then density values, could also be easily estimated using 1D numerical simulation, with a quite good accuracy (i.e., less than the distribution width $\delta R/R$). One should note that the validity of this procedure was only demonstrated with homogeneous jets obtained with conical nozzle geometry. Two-dimensional simulations were still necessary in order to get cluster spatial information. They were validated by the Mach-Zehnder and Rayleigh experiments, with some reserve for the Laval nozzle. In that case, gas expansion was dominated by shock waves. Their major contribution to a decrease of condensation occurred as they converged on the jet axis. This process might be very sensitive to 3D nozzle structures, which could explain the observed discrepancy between 2D calculations and experiments for the Laval nozzle.

Clusters are statistically distributed in size. In the range investigated, distribution width $\delta R/R \sim 15\%$ was inferred from moments calculated by Eqs. (3)–(8). This value is quite small compared to different theoretical estimations [1,28], but comparable with the Mie scattering measurements performed with very large clusters [29]. The ratio $\tilde{N}/N$ depends on the statistical distribution of cluster radius. In the preceding section, it was set to unity. Considering $\delta R/R \sim 15\%$ and assuming a Gaussian distribution, $\tilde{N}/N \sim 1.2$, implying that the experimentally determined value $\tilde{N}$ overestimates N by 20%, which is close to the experimental error bar (cf. Fig. 3). As N is proportional to R^3, only 7% overestimating should be expected on the radius. This is relatively small compared to the distribution width.

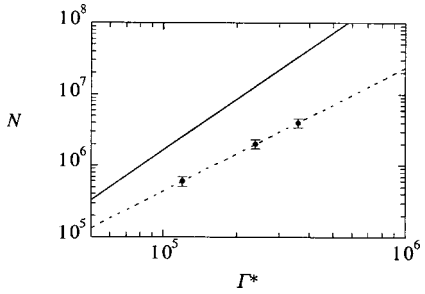

FIG. 5. Number N of atoms per cluster as a function of the Hagena parameter Γ^*. Full line: from the Hagena empirical formula. Full circles: from calculations based on the model presented in Sec. IV. Dotted line: power-law fit of calculated data.

Values of N obtained from calculations for the conical nozzle and confirmed by experiments are plotted in Fig. 5 as a function of the parameter Γ^* introduced by Hagena [9]. These values were averaged over the jet section, at 1.5 mm from the nozzle output, and with backing pressures $P_0 = 20$, 40, and 60 bars. The Hagena empirical formula given by

$$N = 33\left(\frac{\Gamma^*}{1000}\right)^{2.35} \tag{15}$$

is plotted in the same figure (full line). Data were well fitted by similar power scale law, but with different parameters (dotted line):

$$N = 100\left(\frac{\Gamma^*}{1000}\right)^{1.8}. \tag{16}$$

As a consequence, Γ^* was still observed to be a relevant parameter to estimate the average number N of atoms per cluster, but the power factor was observed to be lower than Hagena's value. It is interesting to note that these two laws cross for $\Gamma^* \sim 10^4$, which was the upper value of Γ^* for which the Hagena formula was experimentally validated [9,13]. These results suggest that the Hagena empirical formula (15) should be continued by Eq. (16) in the range of Γ^* from 10^4 to 10^6. Further work will be performed in this direction with a wider range of nozzle parameters, and cluster jet geometry.

IX. CONCLUSION

A two-dimensional numerical model was developed in order to calculate gas expansion and condensation through supersonic nozzles. Total atomic density, condensation rate, cluster size, and density were derived from this model with spatial transverse resolution in a stationary regime. Nozzles with different geometry (Laval and conical) were studied.

Two independent optical diagnostics were developed to validate this model, both with spatial resolution through the gas and cluster jet. Mach-Zehnder interferometry directly led to the measurement of total atomic density N_{tot} in very good agreement with calculations. A simple analytical 1D calculation was observed to give a good estimate of N_{tot}. The product of the condensation rate and the average number of atoms per cluster was deduced from the Rayleigh scattering experiments. A good general agreement was observed for the cluster spatial distribution at the nozzle output. Some discrepancy in the absolute values was, however, observed with the Laval nozzle, within a factor of 2. This could be due to high sensibility of gas cooling strongly affected by 3D shock waves with this geometry. With the conical geometry, this effect was less relevant for cluster production. Homogeneous gas and cluster jets were obtained both experimentally and numerically. It was demonstrated that lower cost 1D simulations were well suited to estimate cluster size and density at the nozzle output. High-density cluster jets ($\sim 10^{12}$ clusters per cm^3) were produced and characterized with adjustable average radius R from 180 to 350 Å with backing pressure from 20 to 60 bars. Statistical distribution width $\delta R/R$ about 15% was inferred from calculations. These results were compared with the Hagena empirical formula, which has been experimentally validated for small clusters. Discrepancy was observed, suggesting that this formula should be modified in this range of large clusters.

ACKNOWLEDGMENTS

This work was partially supported by the Fond Européen de Développement Economique Régional, the Conseil Régional d'Aquitaine, the Russian Foundation for Basic Research (Project No. 02-01000708), and the CRDF project RP1-2328-ME-02.

[1] V. P. Krainov and M. B. Smirnov, Phys. Rep. **370**, 237 (2002).
[2] J. Zweiback, T. Ditmire, and M. D. Perry, Phys. Rev. A **59**, R3166 (1999).
[3] T. Ditmire, E. T. Gumbrell, R. A. Smith, A. Djaoui, and M. H. R. Hutchinson, Phys. Rev. Lett. **80**, 720 (1998).
[4] T. Ditmire, T. Donnelly, R. W. Falcone, and M. D. Perry, Phys. Rev. Lett. **75**, 3122 (1995).
[5] T. Ditmire, J. Zweiback, V. P. Yanovsky, T. E. Cowan, G. Hays, and K. B. Wharton, Nature (London) **398**, 489 (1999).
[6] G. D. Kubiak, L. J. Bernardez, K. D. Krenz, D. J. O'Connell, R. Gutowski, and A. M. Todd, OSA Trends Opt. Photonics Ser. **4**, 66 (1996).
[7] S. Montero *et al.*, in *Atomic and Molecular Beams*, edited by R. Campargue (Springer, Berlin, 2001), p. 295.
[8] O. F. Hagena, Z. Phys. D: At., Mol. Clusters **4**, 291 (1987).
[9] O. F. Hagena, Rev. Sci. Instrum. **63**, 2374 (1992).
[10] J. Farges, M. F. De Feraudy, B. Raoult, and G. Torchet, Surf. Sci. **106**, 95 (1981).
[11] U. Buck and R. Krohne, J. Chem. Phys. **105**, 5408 (1996).
[12] A. J. Bell, J. M. Mestdagh, J. Berlande, X. Biquard, J. Cuvellier, A. Lallement, P. Meynadier, O. Sublemontier, and J. P. Visticot, J. Phys. D **26**, 994 (1993).
[13] A. M. Bush, A. J. Bell, J. G. Frey, and J. M. Mestdagh, J. Phys. Chem. A **102**, 6457 (1998).
[14] R. A. Smith, T. Ditmire, and J. W. G. Tisch, Rev. Sci. Instrum. **69**, 3798 (1998).
[15] A. S. Boldarev, V. A. Gasilov, F. Blasco, Ch. Stenz, F. Dorchies, F. Salin, A. Ya. Faenov, T. A. Pikuz, A. I. Magunov, and I. Yu. Skobelev, JETP Lett. **73**, 514 (2001).
[16] I. Yu. Skobelev, A. Ya. Faenov, A. I. Magunov, T. A. Pikuz, A. S. Boldarev, V. A. Gasilov, J. Abdallah, Jr., G. C. Junkel-Vives, T. Auguste, P. d'Oliveira, S. Hulin, P. Monot, F. Blasco, F. Dorchies, T. Caillaud, C. Bonte, Ch. Stenz, F. Salin, and B. Yu. Sharkov, JETP **94**, 73 (2002).
[17] J. Farges, M. F. De Feraudy, B. Raoult, and G. Torchet, Surf. Sci. **106**, 95 (1981).
[18] General Valve Corporation®.
[19] L. Prandtl, in *Précis de Mécanique des Fluides* (Dunod, Paris, 1940).
[20] F. F. Abraham, *Homogeneous Nucleation Theory* (Academic, New York, 1974).
[21] L. S. Bartell, J. Phys. Chem. **94**, 5102 (1990).
[22] S. M. Kathmann, G. K. Schenter, and B. C. Garett, J. Chem. Phys. **111**, 4688 (1999).
[23] Ya. I. Frenkel, *Kinetic Theory of Liquids* (Nauka, Leningrad, 1975).
[24] V. Malka, C. Coulaud, J. P. Geindre, V. Lopez, Z. Najmudin, D. Neely, and F. Amiranoff, Rev. Sci. Instrum. **71**, 2329 (2000).
[25] *Atomic, Molecular and Optical Physics Handbook*, edited by Gordon W. Drake (Springer-Verlag, New York, 1996).
[26] M. Born and E. Wolf, *Principles of Optics*, 6th ed. (Cambridge University Press, Cambridge, 1980).
[27] J. W. Strutt (Lord Rayleigh), Philos. Mag. **41**, 447 (1871).
[28] M. A. Ratner, Low Temp. Phys. **25**, 266 (1999).
[29] E. T. Gumbrell, A. J. Comley, M. H. R. Hutchinson, and R. A. Smith, Phys. Plasmas **8**, 1329 (2001).